NATIONAL AERONAUTICS AND SPACE ADMINISTRATION

Technical Memorandum 33-740

In-Flight Calibration of the High-Gain Antenna Pointing for the Mariner Venus-Mercury 1973 Spacecraft

J. M. Herdman

W. F. Havens

H. Ohtakay

JET PROPULSION LABORATORY

CALIFORNIA INSTITUTE OF TECHNOLOGY

PASADENA, CALIFORNIA

October 15, 1975

1. Report No. 33-740	2. Government Accession No.	3. Recipient's Catalog No.
4. Title and Subtitle IN-FLIGHT CALIBRATION OF THE HIGH-GAIN ANTENNA POINTING FOR THE MARINER VENUS-MERCURY 1973 SPACECRAFT		5. Report Date October 15, 1975
		6. Performing Organization Code
7. Author(s) J. M. Hardman, W. F. Havens, H. Ohtakay		8. Performing Organization Report No.
9. Performing Organization Name and Address JET PROPULSION LABORATORY California Institute of Technology 4800 Oak Grove Drive Pasadena, California 91103		10. Work Unit No.
		11. Contract or Grant No. NAS 7-100
		13. Type of Report and Period Covered Technical Memorandum
12. Sponsoring Agency Name and Address NATIONAL AERONAUTICS AND SPACE ADMINISTRATION Washington, D.C. 20546		
		14. Sponsoring Agency Code

15. Supplementary Notes

16. Abstract

The methods used to in-flight calibrate the pointing direction of the Mariner Venus-Mercury 1973 spacecraft high gain antenna and the achieved antenna pointing accuracy are described. The overall pointing calibration was accomplished by performing calibration sequences at a number of points along the spacecraft trajectory. Each of these consisted of articulating the antenna about the expected spacecraft-earth vector to determine systematic pointing errors. The high gain antenna pointing system, the error model used in the calibration, and the calibration and pointing strategy and results are discussed.

17. Key Words (Selected by Author(s)) Spacecraft Design, Testing and Performance Systems Analysis Mariner Venus/Mercury 1973 Project	18. Distribution Statement Unclassified -- Unlimited

19. Security Classif. (of this report) Unclassified	20. Security Classif. (of this page) Unclassified	21. No. of Pages 34	22. Price

HOW TO FILL OUT THE TECHNICAL REPORT STANDARD TITLE PAGE

Make items 1, 4, 5, 9, 12, and 13 agree with the corresponding information on the report cover. Use all capital letters for title (item 4). Leave items 2, 6, and 14 blank. Complete the remaining items as follows:

3. Recipient's Catalog No. Reserved for use by report recipients.

7. Author(s). Include corresponding information from the report cover. In addition, list the affiliation of an author if it differs from that of the performing organization.

8. Performing Organization Report No. Insert if performing organization wishes to assign this number.

10. Work Unit No. Use the agency-wide code (for example, 923-50-10-06-72), which uniquely identifies the work unit under which the work was authorized. Non-NASA performing organizations will leave this blank.

11. Insert the number of the contract or grant under which the report was prepared.

15. Supplementary Notes. Enter information not included elsewhere but useful, such as: Prepared in cooperation with... Translation of (or by)... Presented at conference of... To be published in...

16. Abstract. Include a brief (not to exceed 200 words) factual summary of the most significant information contained in the report. If possible, the abstract of a classified report should be unclassified. If the report contains a significant bibliography or literature survey, mention it here.

17. Key Words. Insert terms or short phrases selected by the author that identify the principal subjects covered in the report, and that are sufficiently specific and precise to be used for cataloging.

18. Distribution Statement. Enter one of the authorized statements used to denote releasability to the public or a limitation on dissemination for reasons other than security of defense information. Authorized statements are "Unclassified—Unlimited, " "U. S. Government and Contractors only, " "U. S. Government Agencies only, " and "NASA and NASA Contractors only. "

19. Security Classification (of report). NOTE: Reports carrying a security classification will require additional markings giving security and down-grading information as specified by the Security Requirements Checklist and the DoD Industrial Security Manual (DoD 5220.22-M).

20. Security Classification (of this page). NOTE: Because this page may be used in preparing announcements, bibliographies, and data banks, it should be unclassified if possible. If a classification is required, indicate separately the classification of the title and the abstract by following these items with either "(U)" for unclassified, or "(C)" or "(S)" as applicable for classified items.

21. No. of Pages. Insert the number of pages.

22. Price. Insert the price set by the Clearinghouse for Federal Scientific and Technical Information or the Government Printing Office, if known.

PREFACE

The work described in this report was performed by the Guidance and Control Division of the Jet Propulsion Laboratory, under the cognizance of the Mariner Venus-Mercury 1973 Project.

ACKNOWLEDGEMENT

CONTENTS

ABSTRACT

The methods used to in-flight calibrate the pointing direction of the Mariner Venus-Mercury 1973 spacecraft high gain antenna and the achieved antenna pointing accuracy are described. The overall pointing calibration was accomplished by performing calibration sequences at a number of points along the spacecraft trajectory. Each of these consisted of articulating the antenna about the expected spacecraft-earth vector to determine systematic pointing errors. The high gain antenna pointing system, the error model used in the calibration, and the calibration and pointing strategy and results are discussed.

SECTION I

INTRODUCTION

The Mariner Venus-Mercury 1973 (MVM'73) spacecraft carried a two degree-of-freedom gimbaled high gain antenna (HGA). This HGA was used for two purposes throughout the mission: the transmission of high rate science and engineering telemetry to the Earth, and the Radio Science experiments. The spacecraft had two transmitters, an S-band (2.295 GHz) which carried telemetry data, and an X-band (8.415 GHz) which was modulated by ranging code. Optimum pointing was required at the encounters to support high rate telemetry (117.6 kilobits per second (kbps) at Venus and 22.05 kbps at Mercury) and the dual frequency occultation Radio Science experiments.

Spacecraft system requirements (Reference 1) did not include a HGA pointing accuracy requirement. However, the desired telecommunications performance described above dictated antenna pointing error be held to less than 1.0 deg, with a goal of pointing error as small as 0.7 deg. In order to achieve this pointing accuracy, an in-flight calibration of HGA pointing was necessary. This calibration was performed using the X-band main lobe because of its narrow beamwidth (the half-beamwidth was 0.9 deg at the 3dB point).

The in-flight calibration was achieved by statistically estimating mechanical, electronic and electromagnetic errors arising in sensors, antenna structures and antenna radiation patterns during flight. Because the HGA boresight pointing error can only be measured with respect to the spacecraft-Earth direction, many calibration sequences were required to characterize and compensate for these errors over an extended range. This dictated a calibration strategy which called for several calibrations space in time to cover a wide range of HGA directions.

SECTION II
HIGH GAIN ANTENNA POINTING SYSTEM

The high gain antenna pointing relative to the Mariner 10 spacecraft
was accomplished by articulating the antenna dish about its two control axes.
A three-axis stabilized spacecraft orientation was maintained by a cold
gas reaction control system utilizing celestial sensor error signals, inertial
gyro error signals or a combination of the two systems. A view of the space-
craft and the HGA as given in Figure 1.

After spacecraft launch, the HGA boom was deployed to a predetermined
nominal position, which allowed the dish to point in all directions except
those obscured by the spacecraft. The Articulation and Pointing Subsystem (APS),
which controlled the pointing relative to the spacecraft, was comprised of
two independent actuators, boom and dish, and associated electronics. The
boom actuator was mounted at the tip of the antenna boom which remained
in a fixed orientation relative to the spacecraft after deployment. The
dish actuator was mounted perpendicular to the boom actuator with the antenna
dish mounted so that the boresight was perpendicular to the dish actuator.

The APS functioned in two modes, Position and Incremental, and at
two actuator slew rates, 0.125 deg/sec and 1.0 deg/sec. In the Position
Mode the actuator could be commanded to any position within its range with
a resolution of 0.125 deg. In the Incremental Mode the actuator could be
slewed a fixed increment as large as 40.92 deg with a resolution of 0.04
deg. A simplified block diagram of APS is given in Figure 2.

Telemetry provided information about spacecraft and HGA angular position.
Telemetry measurements from the celestial sensors provided attitude control
angular position information with a resolution of 0.02 deg in pitch and yaw
and 0.03 deg in roll. Potentiometers geared to the actuator output shafts
provided coarse and fine telemetry measurements with a resolution of 2.0
deg and 0.04 deg, respectively. Additional details on spacecraft mechanization
may be found in Reference 2.

The nominal boom and dish actuator angles to point the antenna in
a desired direction were calculated in the error-free system. Two solutions
(primary and secondary) were possible, subject to constraints imposed by
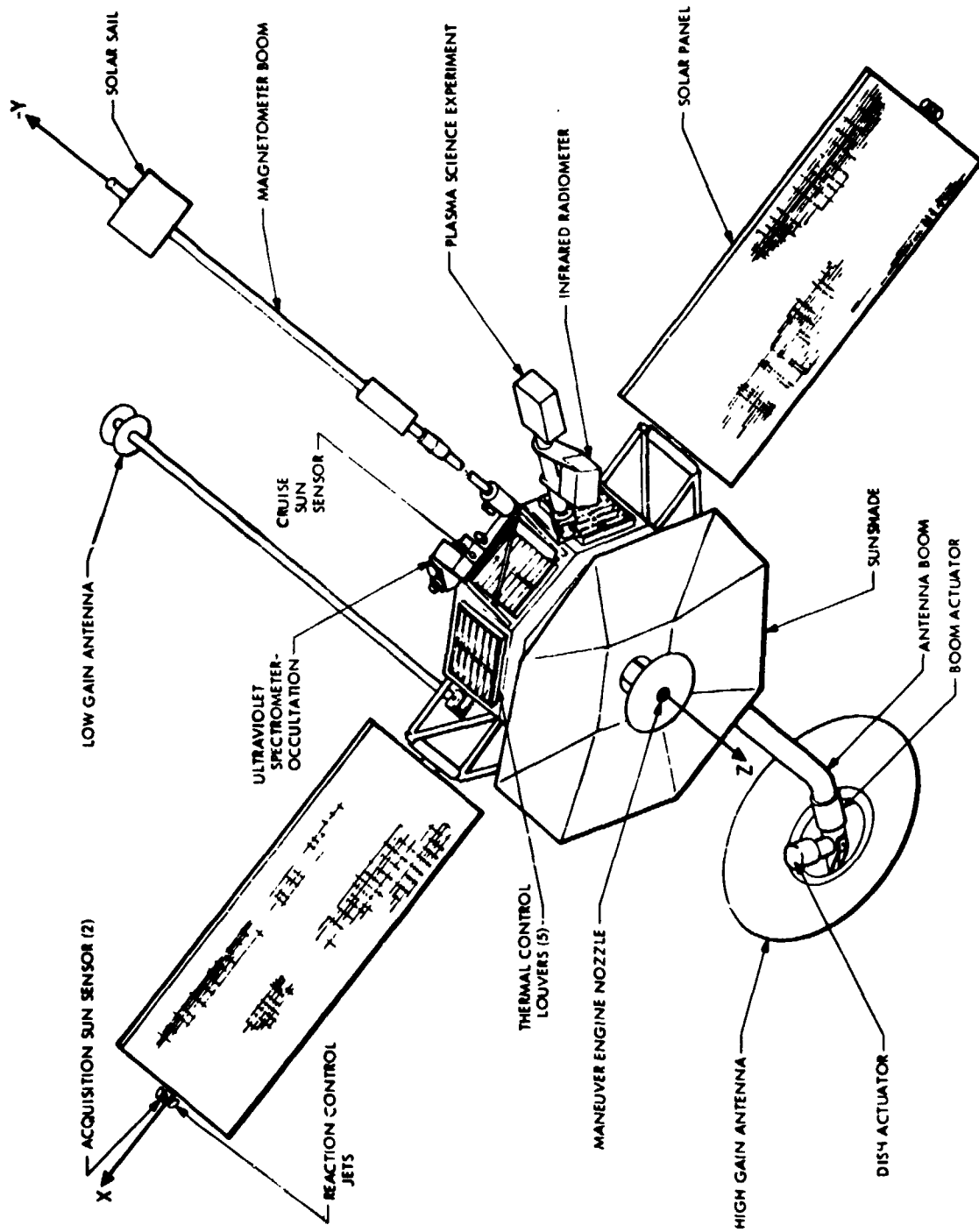
Fig. 1 Mariner Venus Mercury 1973 Spacecraft
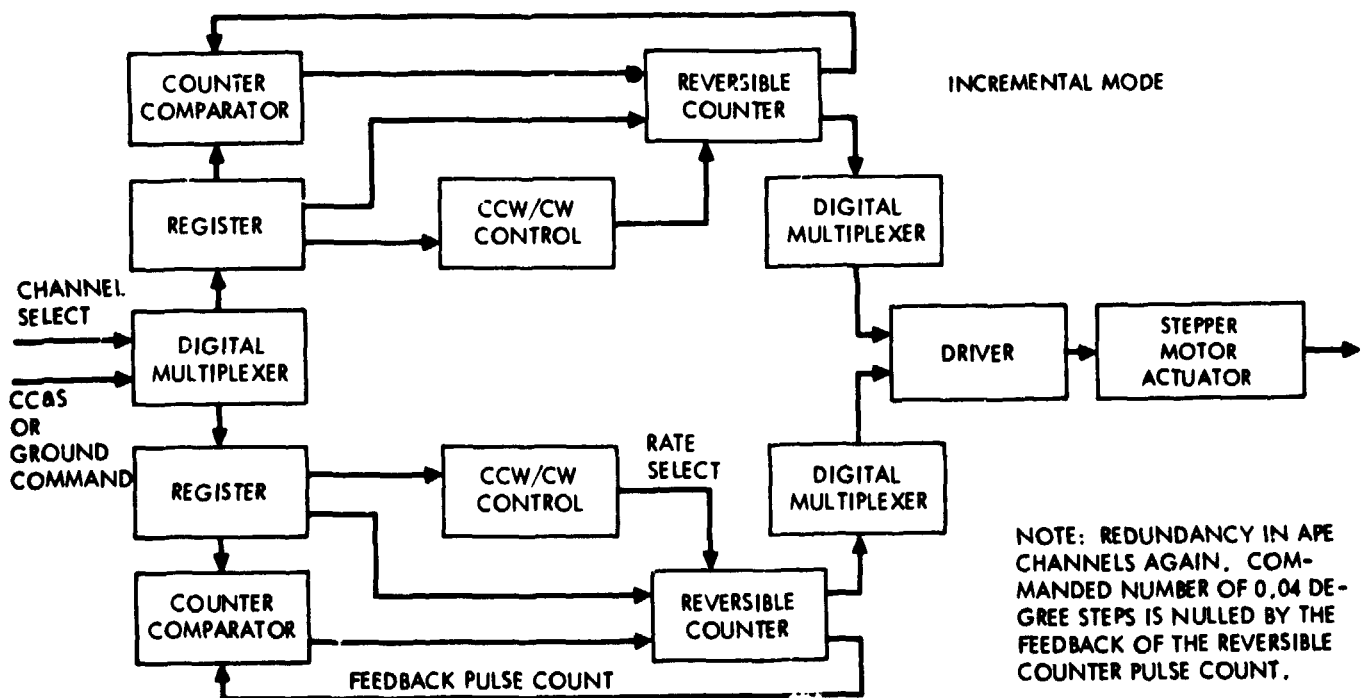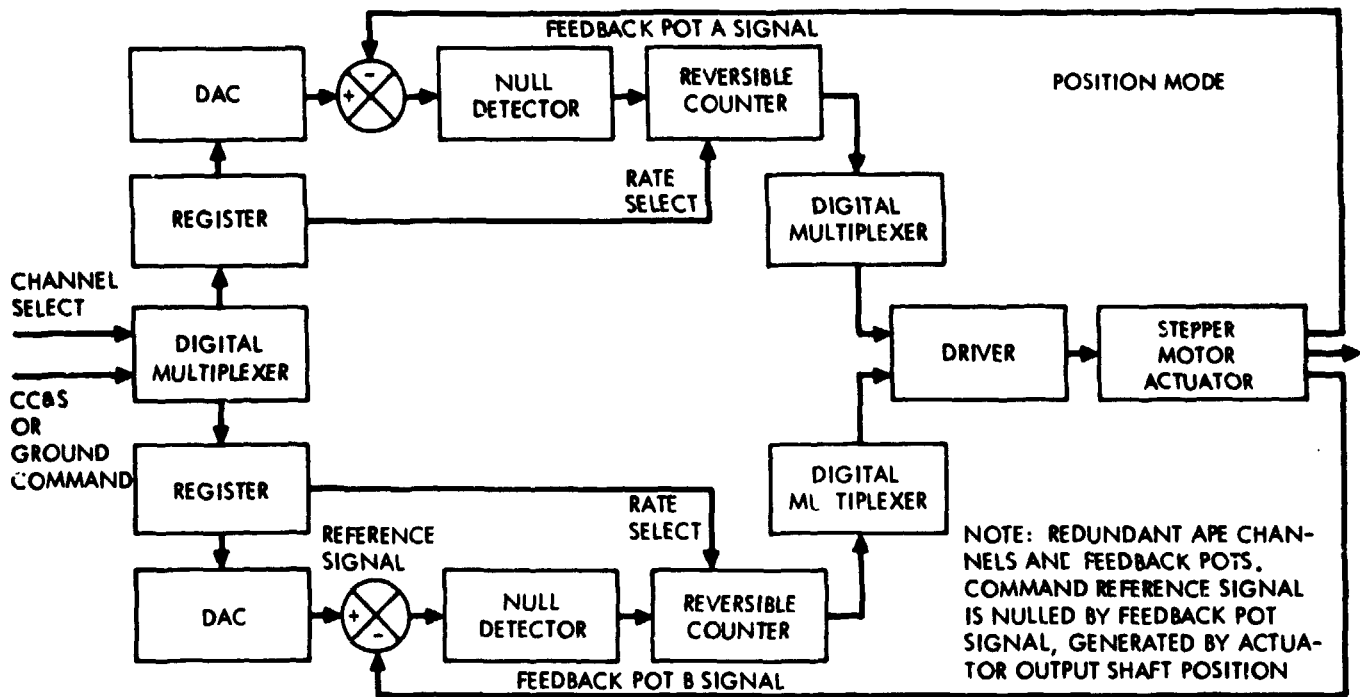
Fig. 2 Simplified APS Block Diagram

the electrical and mechanical configuration of the APS. (These constraints are described in Figure 3.) The actuators were restricted so that the dish actuator output shaft angle must lay between -4.5 and +184.5 deg while boom lay between 0 and 255 deg. Within these constraints there were two boom-dish pairs to point the HGA in many of the desired directions.

By definition the primary solution pair contained dish actuator angles less than 90 deg while the secondary solution pair had dish actuator angles greater than 90 deg. The nominal Earth track in boom and dish for the primary and secondary solutions is illustrated in Figure 3. For the MVM'73 mission, launched November 3, 1973, only the primary solution could have been used in the first 75 days and only the secondary solution could have been used after 135 days. The re-orientation to the secondary solution, called the flip-flop, occurred on day 111, 17 days following Venus encounter.

Fig. 3 Nominal HGA Pointing Configuration
for Boom and Dish Actuators

SECTION III
ERROR SOURCES AND MODELS

Two types of error sources, control and knowledge, should be considered to determine the HGA pointing accuracy. The knowledge-type error sources include antenna structural offset errors, sensor offsets, scale factors and telemetry resolution, and unknown parameters associated with the HGA radiation pattern. Once these error sources and characteristics are identified, the fixed errors can be compens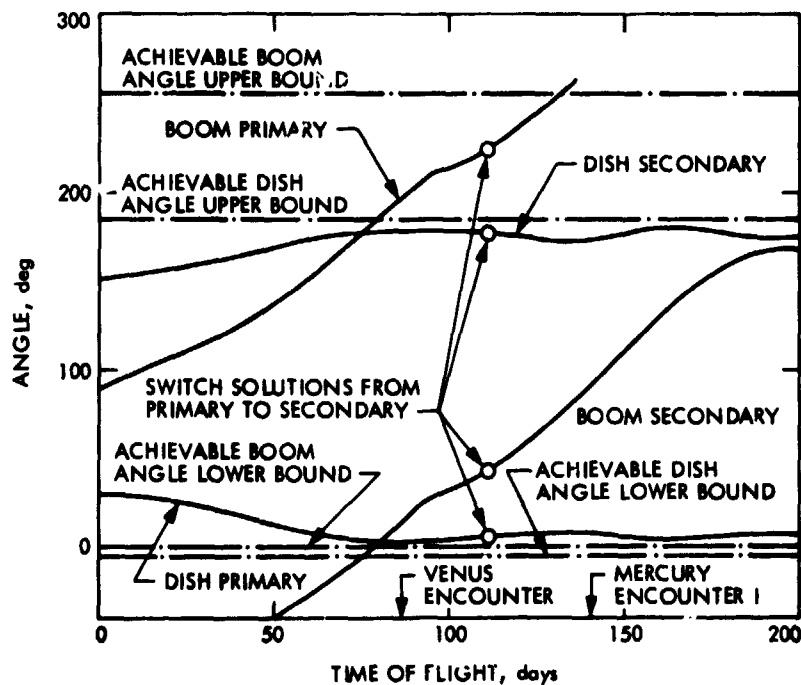ated to enhance the pointing knowledge accuracy. The control-type error sources include limit cycle motion of the spacecraft and APS command and execution resolution. In the following, the knowledge-type error sources are identified and characterized through mathematical models.

The in-flight calibration of the HGA pointing required establishing an analytic model of the HGA radiation pattern. An accurate mathematical model of the peak of the X-band main lobe was developed. Calibration measurements were planned only for the main lobe which ranged about two degrees from the antenna boresight (or equivalently from 0 to -10 dB in the signal strength measurements). The main lobe radiation pattern was modeled by:

$$G(\theta) = k_1 \left(\frac{\sin k_2 \theta}{\theta} \right)^2 \tag{1}$$

where

k_1 = antenna gain constant

k_2 = radiation pattern constant

θ = antenna cone angle.

The signal strength measured at the ground station from an antenna whose boresight lay off the Earth by the angle θ is proportional to:

$$S(\theta) = 10 \log_{10} G(\theta) \tag{2}$$

The feasibility of this model was examined against the accurately measured radiation pattern of the HGA prior to launch. Discrepancies between the model and the measured radiation pattern in the main lobe were confirmed

to be less than 0.1 dB (1σ) and were treated as a part of the measurement
noise. The Automatic Gain Control (AGC) bias of the receiving station provided
voltages proportional to the signal strength of S- and X-band carrier frequencies
averaged over five-second intervals (see Reference 3). The voltages were
multiplied by appropriate scale factors for conversion into dB, then quantized.

The HGA cone angle, θ, was determined using the spacecraft-Earth vector
and the vector parallel to the HGA radiation beam. Ground-based radio orbit
determination provided a spacecraft-Earth vector, $\hat{v}_E$, which was then expressed
in the antenna coordinate system. This was accomplished through successive
transformations of $\hat{v}_E$ in various spacecraft structure-fixed coordinate systems.
These coordinate systems and transformation matrices are described in detail
in Reference 4. They are summarized in Table 1. The subsequent discussion
is concerned with investigation of error sources which are assumed to be
time invariant once the spacecraft is launched.

The true coordinate systems, in general, differ from the nominal
systems due to errors (denoted by z's) caused by spacecraft-navigation residual
errors, errors arising in various onboard sensor electronics and telemetry
channels, mechanical misalignments introduced during spacecraft fabrication
and caused by gravitational environment change, and deformation of radiation
pattern of the HGA. The composite effects of these errors may be completely
represented by a skew symmetric matrix

$$
E = \begin{bmatrix} 0 & \varepsilon_3 & -\varepsilon_2 \\ -\varepsilon_3 & 0 & \varepsilon_1 \\ \varepsilon_2 & -\varepsilon_1 & 0 \end{bmatrix} \tag{3}
$$

provided ε's are small. Elements of this matrix are expressed in terms of
individual error sources:

$$
\text{col} (\varepsilon_1, \varepsilon_2, \varepsilon_3) = \sum_{i=1}^{5} T_{5i} \, \bar{e}_i \tag{4}
$$

where

　　T = coordinate transformation matrix (see Table 1)

　　$\bar{e}$ = error parameter vector

Table 1 Spacecraft and HGA Structure Coordinate Systems

Designation		Description	Definition	Transformation Matrix
Number	Symbol			
0	A	Spacecraft-centered celestial abc	See Figure 4	
	X	S/C XYZ before attitude control limit cycle motion	Rot $(\alpha_x, 3)$ from A, $\alpha_x = -60$ deg	T_{01}
1	X'	S/C XYZ after attitude control limit cycle motion (=X'Y'Z')	Rot $(\phi_r, 3)$ Rot $(\phi_y, 2)$ Rot $(\phi_p, 1)$ from X	
	A'	S/C body fixed abc (= a'b'c')	Rot^{-1} $(\alpha_x, 3)$ from X'	T_{12}
2	K	HGA zero reference after clock angle setting	Rot $(\alpha, 3)$ from A'	
3	N	HGA zero reference after cone angle setting	Rot $(\beta - \frac{\pi}{2}, 2)$ from K	T_{23}
4	B	HGA rotating after boom angle setting	Rot $(\psi_B, 1)$ from N	T_{34}
5	G	HGA coordinate	Rot $(\psi_D, 2)$ from B	T_{45}

Notes: 1. Rot (a, I) defines a positive rotation around the I-th axis by the angle of a.
2. $(\char`\^)$ stands for a unit vector.
3. $T_{ij} = T_{ik} T_{kj}$, transformation from coordinate system j to coordinate system i.

$$\hat{a} = \hat{b} \times \hat{c}$$
$$\hat{b} = \hat{c} \times \bar{c} / |\hat{c} \times \bar{c}|$$

TO SUN
+Z ROLL $(\hat{c})$

+ CONE ANGLE

TO OBJECT (v_E)

$(\hat{b})$

SPACECRAFT

+ CLOCK ANGLE

+ Y
YAW

TO
CANOPUS
$(\bar{c})$

60°

$(\hat{a})$

+ X PITCH
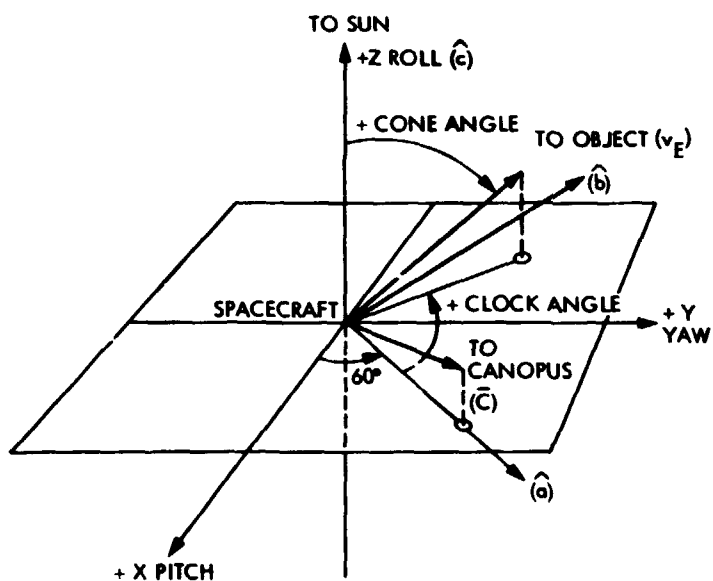
CONE ANGLE OF OBJECT: THE ANGLE FROM THE SPACECRAFT
+ ROLL AXIS TO THE SPACECRAFT/
OBJECT VECTOR

CLOCK ANGLE OF OBJECT: THE ANGLE MEASURED CLOCKWISE
(WHEN LOOKING IN THE + ROLL
DIRECTION) FROM THE SPACECRAFT
ROLL AXIS/CANOPUS TRACKER
PLANE TO THE SPACECRAFT ROLL
AXIS/OBJECT PLANE

Fig. 4 Celestial Coordinate System for
Spacecraft Attitude Control

Furthermore, θ is also given in terms of individual error parameters

$$\theta = \cos^{-1} (\hat{\xi} \; \hat{\zeta}) \qquad (5)$$

where

$\hat{\zeta}$ = HGA boresight unit vector $\underline{\Delta}$col$(0,0,1)$

and

$\hat{\xi}$ = spacecraft-Earth direction in HGA coordinates

The spacecraft-Earth direction is given by

$$\bar{\xi} = (I+E)T_{50}\hat{\nu}_E \qquad (6)$$

in the HGA coordinate system, where

$\hat{\nu}_E$ = spacecraft-Earth unit vector in the spacecraft-centered celestial coordinate system.

Since $\hat{\zeta}$ is a known quantity, the rest of this section describes the error sources which constitute the error vectors $\bar{e}$'s.

The spacecraft body-fixed a'b'c' coordinate system deviates from the celestial abc coordinate system because of spacecraft rotation within the deadband of the attitude control system.

The telemetry of pitch, yaw and roll attitude angles differs from the true values. The attitude sensor null offsets are the dominant error sources in the error vector $\bar{e}_1$

$$\bar{e}_1 = \mathrm{col}(z_1, \; z_2, \; z_3 + z_1\cos\alpha_x\cot\beta_s - z_2\sin\alpha_x\cot\beta_s) \qquad (7)$$

where

α_x = clock angle of spacecraft + X axis (-60 deg for MVM'73),

β_s = cone angle of reference star

The descriptions of the z's are summarized in Table 2.

The true boom deployed configuration deviated slightly from what had been planned due to fabrication error and deployment in almost zero gravity environment. The deviations are represented by

$$\bar{e}_2 = col(0, 0, z_4) \tag{8}$$

and

$$\bar{e}_3 = col(0, z_5, 0) \tag{9}$$

Two error sources associated with the boom actuator were considered. One, z_6, was nonorthogonality between the boom and dish actuator axes, resulting from fabrication error. The other error, z_7, was a discrepancy between telemetered boom angle and its true value, which included boom actuator potentiometer null offset, actuator mechanical backlash, and telemetry data resolution error.

$$\bar{e}_4 = col(z_7, 0, z_6) \tag{10}$$

In defining the true antenna coordinate system two error sources were investigated. Nonorthogonality among axes in the antenna coordinate system can be adjusted by a small angle z_8. The telemetered dish angle value could be different from its true value. The error denoted by z_9 includes dish potentiometer null offset, data resolution, and actuator mechanical backlash.

$$\bar{e}_5 = col(z_8, z_9, 0) \tag{11}$$

The error sources arising in ground station signal processing were mostly electronic and electro-magnetic in nature. The unknown parameter, denoted by z_{10}, includes DC bias drift in AGC electronics, time averaging error of signal strength measurement, and discrepancy of radio signal space loss constant from its nominal value. This error takes a different value at each calibration. The HGA radiation pattern width parameter varied as a function of environmental change. Hence, this parameter, being redefined as

$$z_{11} = k_2 \tag{12}$$

Table 2 Error Sources and Error Parameters

Parameter Identification	Error Sources and Unknown System Parameters	Subsystem
z_1	Pitch sensor null offset	Attitude Control Subsystem
z_2	Yaw sensor null offset	Attitude Control Subsystem
z_3	Roll sensor null offset	Attitude Control Subsystem
z_4	Boom axis clock angle mounting misalignment	Structures Subsystem
z_5	Boom axis cone angle mounting misalignment	Structures Subsystem
z_6	Boom-Dish axes non-orthogonality	Structures Subsystem
z_7	Boom actuator mechanical and potentiometer null offset	Articulation and Pointing Subsystem
z_8	Dish-HGA boresight non-orthogonality	Structures Subsystem
z_9	Dish actuator mechanical and potentiometer null offset	Articulation and Pointing Subsystem
z_{10}	HGA radiation beam width	HGA Subsystem
z_{11}	AGC Bias. HGA radiation pattern gain constant	HGA Subsystem/Signal Strength Measurement Subsystem

was included among the error parameters being solved for. Spacecraft navigation errors were insignificant contributors to the HGA pointing error.

The random noise power components denoted by η additive to the signal strength measurements were contributed by two sources: one was inherent to the receiving antenna environment and the other was indirectly introduced, through the computation of expected signal strength, from engineering telemetry noise and the onboard antenna modeling residual errors. The antenna-originated noise is generally known in terms of noise temperature and is due to electromagnetic radiation generated by celestial bodies within the antenna beam, atmospheric absorption and reradiation, and absorption and reradiation by physical bodies surrounding the antenna. The weather-induced noise temperature of the Deep Space Network (DSN) antenna when it is aimed at cold sky, i.e., no major celestial sources around the antenna boresight, is given in Reference 5. The predicted antenna noise temperature for the period of November 1973 through March 1974 based upon the past observation data was 35° Kelvin or equivalently 0.14 dB (1σ). Random noise, assumed to be normally distributed, in attitude and actuator angle telemetry measurements mapped into noise in expected value of signal strength measurements. The HGA modeling residual errors, measured to be less than 0.1 dBm at pre-launch calibration, were also added to the random noise in the signal strength measurement model.

From Eqs. (1) through (12), one can express the expected signal strength measurement value in terms of individual error parameters and the system parameters (see Table 2)

$$S = S(z_i, T_{5j}:t) + \eta(t)$$

where

$$i = (1,2,\ldots,11)$$
$$j = (1,2,\ldots,5)$$

Among the system parameters, which uniquely defined the orthogonal transformation T_{5j}'s (see Table 1), α_x, α and β stayed constant throughout the spacecraft flight, while ψ_D, ψ_B, ϕ_p, ϕ_y and ϕ_r were obtained via engineering telemetry channels and β_s from results of spacecraft orbit determination.

The difference between the observed signal strength and expected signal strength, S_{ob} and S, respectively, can be approximated by a linear function of perturbation, δz, of the unknown parameters:

$$\delta S = S_{ob} - S$$

$$= \frac{\partial S}{\partial z} \, \delta z + \eta$$

where

$\frac{\partial S}{\partial z}$ is evaluated at the most updated values of parameters.

Hence, a use of the Kalman filter algorithm enables solution for the unknown error parameters z_i's, treating Eq. (13) as the observation equation.

SECTION IV
IN-FLIGHT CALIBRATION STRATEGY AND EXECUTION

The in-flight calibration was planned based upon computer simulations conducted prior to launch. The basic planning philosophy was the following:

(1) Calibrations be distributed widely in time so that the greatest range of actuator angles could be covered. This was intended to produce a uniform HGA pointing accuracy over the widest available range of actuator angles and to obtain better estimates of error parameters with small correlations.

(2) At least one calibration be performed close to each of the critical periods of the mission, i.e., encounter with the target planets, which would insure a high pointing accuracy throughout such critical periods.

(3) Calibrations be conducted without interference with the other mission activities having higher priority.

The original schedule called for eleven calibrations, six before Venus encounter and five between Venus and Mercury. The actual number of useful calibrations performed during the mission was nine, four before Venus encounter. Station data problems and spacecraft problems each eliminated one calibration. The calibrations were performed during Deep Space Station (DSS) 14 tracking since this 64-meter antenna was the only one in the DSN with X-band capability. The actual schedule is shown in the Appendix. Operational aspects of calibration planning which were considered include the following:

(1) Meeting the desired pointing accuracy during critical periods of the mission.

(2) Adequate time for data processing prior to major updates of the HGA pointing profile.

(3) Contingency calibrations for covering problems which might invalidate a critical calibration.

(4) Manpower and training for the smooth operation of the calibration sequence and data processing.

(5) Full checkou_ of the facilities and software before testing and training.

The lead time for major mission sequence updates for the MVM mission was fourteen working days which included four days for calibration processing for final corrections and ten days for sequence implementation. Due to operational constraints, the HGA profile was not redesigned during the mission but was corrected by a small translation of the total profile in both boom and dish after the first calibration. This was deemed sufficient for cruise (S-band) operations. During critical periods for the Radio Science experiment, the latest available pointing profile was used for ground commanding the HGA.

Each calibration was performed by pointing the HGA nominally at Earth and then moving it in a box pattern and measuring signal strength variations at several points on the box. In this manner the X-band main lobe was moved such that the Earth received signal strength varied significantly. Analysis of these data revealed the true position of the Earth in antenna coordinates.

The initial calibration pattern is shown in Figure 5. The box is plotted in gimbal coordinates for the ten slews. Next to it are tabulated the commands and resulting actuator-angle deltas for the slews. The terminology CWI 18 means the actuator was slewed clockwise in the Incremental Mode 18 steps of 0.04 deg each (0.72 deg total). Following set-up slews to take out backlash and point in the expected Earth direction, the actuators were slewed to each of the positions. The actuator-internal backlash was expected to be 0.16 deg, so when a change in direction occurred, four additional steps were included.

Analysis of the first two calibrations indicated a substantial amount of backlash existed in both the boom and dish linkages between the actuator output shaft and the antenna. To avoid degradation in calibration data quality and to evaluate the magnitude of the backlash, two new patterns were developed to produce data on this "actuator-external" backlash. These patterns were used beginning with the third calibration. One is illustrated in Figure 6.

Position	Δ Boom		Δ Dish	
1	–		–	
2	CWI 18	– .72 deg	–	
3	–		CWI 18	+ .72 deg
4	CCWI 22	.88	–	
5	CCWI 18	.72	–	
6	–		CCWI 22	– .88
7	–		CCWI 18	– .72
8	CWI 22	– .88	–	
9	CWI 18	– .72		
10	–		CWI 22	.88
11	CCWI 22	.88		

Fig. 5   Initial HGA Calibration Pattern

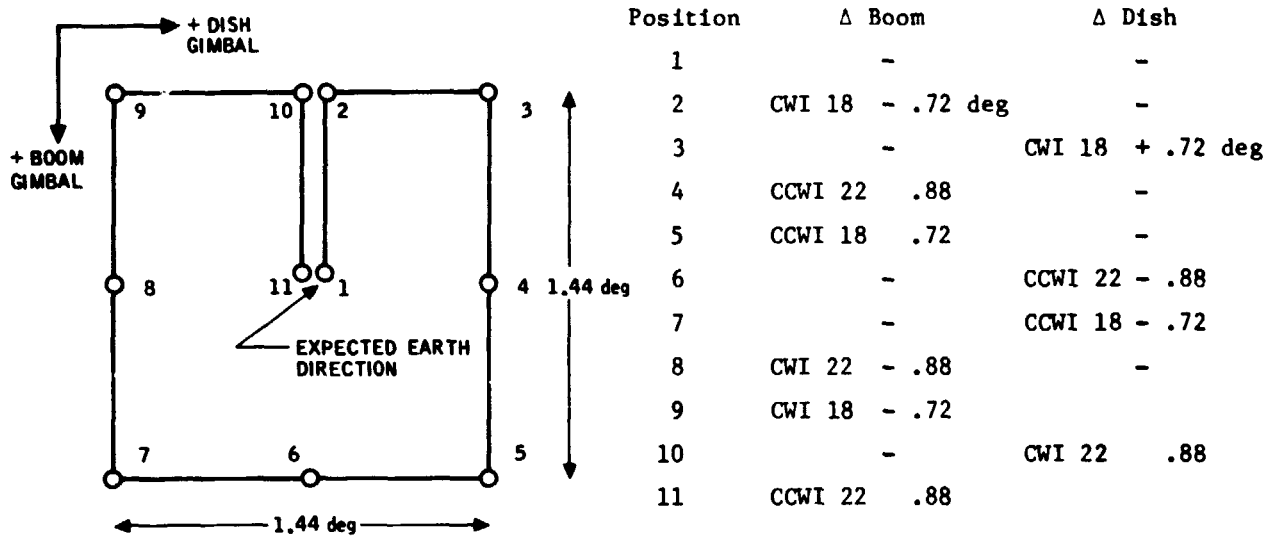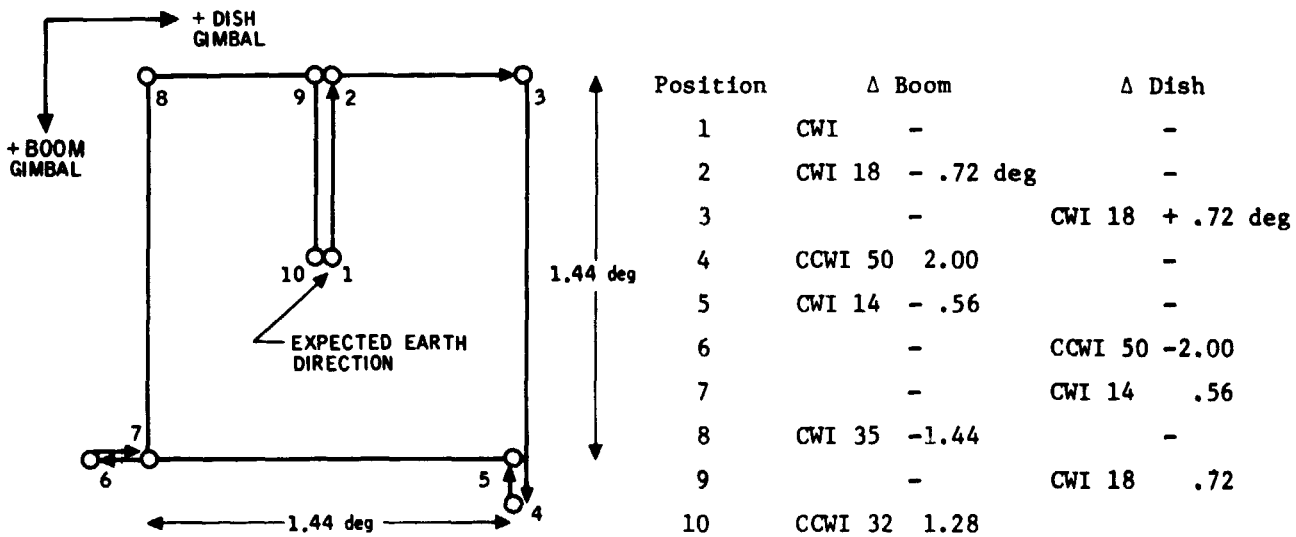| Position	Δ Boom		Δ Dish	
1	CWI	–	–	
2	CWI 18	– .72 deg	–	
3	–		CWI 18	+ .72 deg
4	CCWI 50	2.00	–	
5	CWI 14	– .56	–	
6	–		CCWI 50	-2.00
7	–		CWI 14	.56
8	CWI 35	-1.44	–	
9	–		CWI 18	.72
10	CCWI 32	1.28		

Fig. 6   HGA Calibration Pattern--Revised for Backlash

This approach resulted in a set of signal strength data which were
taken consistently on one side of the backlash hysteresis curves as is illustrated
in Figure 7. The data recorded at positions 1, 2, 3, 5, 7, 8 and 9 were
used for pointing calibration. The data recorded at points 4, 5, 6 and 7
were used for determination of external backlash magnitude.

Typical signal strength measurements for one calibration which took
about forty minutes are shown in Figure 8. Slews were on three-minute centers.
Sharp rises and falls in the signal strength measurements represent transient
responses to commanded slews. A time delay before, and an overshoot after,
a transient response in signal strength measurements, each lasting for five
to ten seconds, were observed. Apparently, the former was caused by a composite
effect of signal lag in AGC electronics and time averaging of signal strength
measurements, and the latter by underdamped characteristics of AGC electronics.
To avoid false measurements, signal strength data immediately before and
after a transient was removed from further processing, resulting in about 2.5
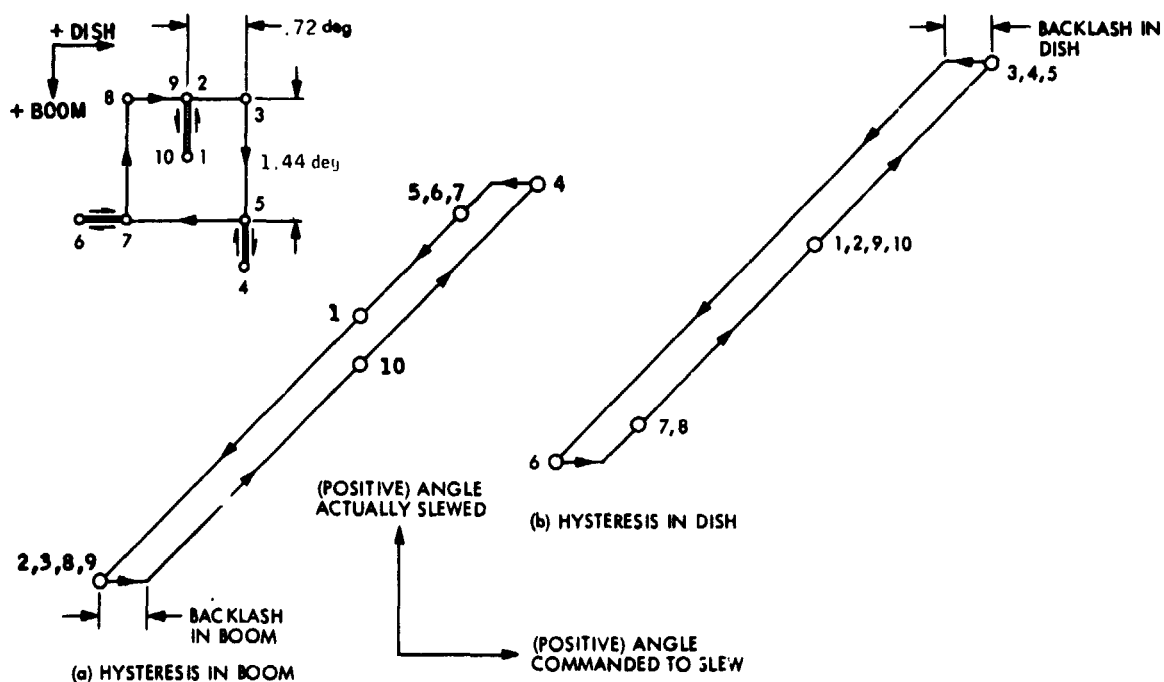minutes of valid data at each measurement point.

Fig. 7 HGA Slew Pattern for Backlash-Free In-Flight
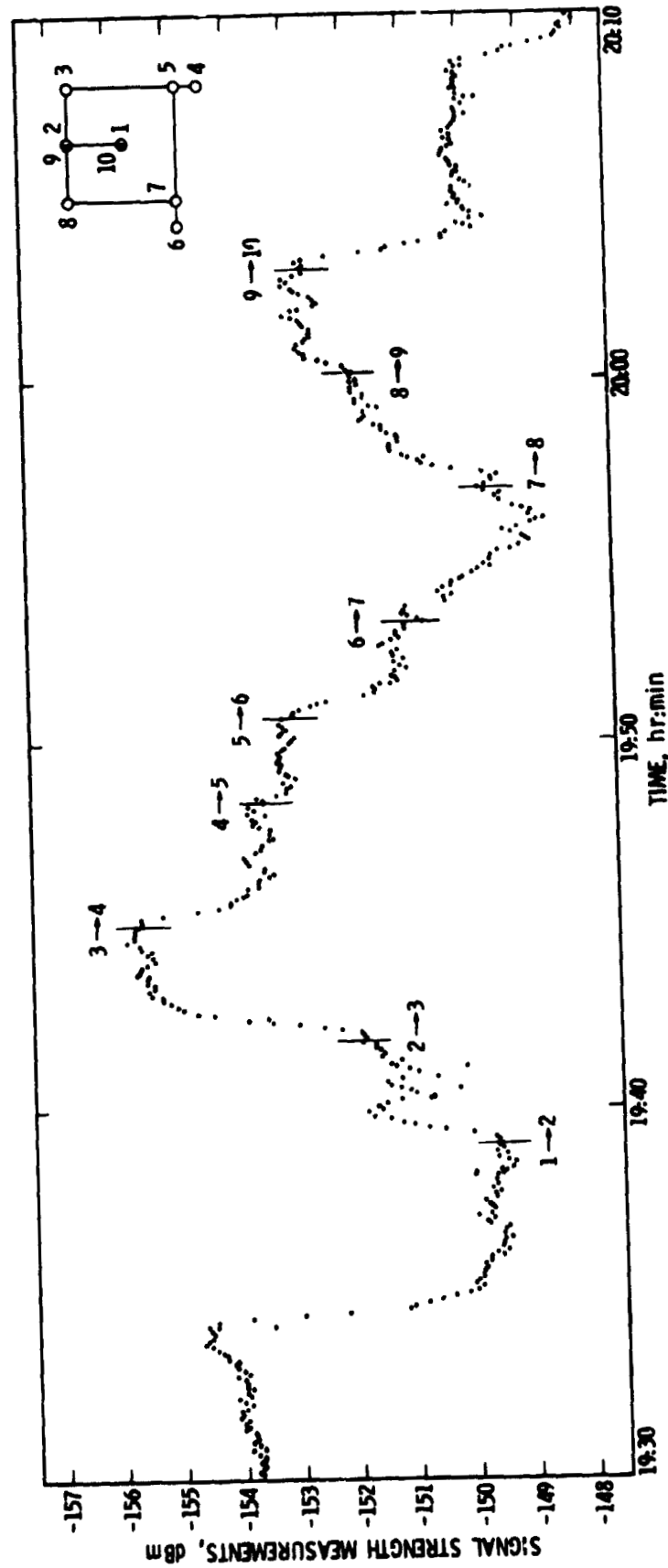Calibration and Hysteresis Curves

Fig. 8 Signal Strength Measurements During In-Flight C--'- ton

SECTION V
IN-FLIGHT CALIBRATION RESULTS

This section presents the results obtaineḽ from analysis of the ꞓalibration data. Estimates of mean and variance of the boom and dish offsets are given graphically for each calibration. These are represented, respectively, by the compensated actuator angles and calibration accuracy. Then at three important epochs, i.e., near Earth, Venus and Mercury, calibration results are tabulated Finally, antenna pointing accuracy is described as a function of mission time. A summary of conclusions and recommendations based on the calibration experience is given.

An understanding of the improved pointing capability resulting from the calibration process may be obtained from inspection of Figure 9. This figure shows directions and magnitudes of actuator gimbal angle compensation immediately after each calibration. The gradual decrease in magnitudes of compensation in the first four calibrations indicates the convergent process of pointing error correction. Calibrations 7 and 8 were done immediately before and after the flip-flop. The increased error in boom gimbal at Calibration 7 is the result of extrapolation beyond the calibrated range achieved 38 days earlier at Calibration 5. The flip-flop represented an even greater excursion beyond the calibrated range. Therefore, accumulated knowledge about the antenna pointing error obtained befor ʰhe flip-flop was thrown out. Subsequent calibrations restored pointing calibration accuracy, resulting in a gradual decrease in magnitudes of angular compensation. Changes in signs of correction angles were caused by possible over-compensation in previous calibrations.

A measure of the increasing accuracy of the estiʋates of the boom and dish offsets during the calibration process is given in Figure 10. Calibration accuracy is the mapping, into the antenna coordinate system, of the effect on boresight pointing accuracy of the eleven parameters being estimated. In this figure, the upward slopes of the curves between two successive calibrations were caused by time-varying elements of pointing accuracy evaluation functions. This may also be explained as a decrease in the level of confidence in pointing the HGA as actuator angles move out of the range over which they had been calibrated. The length of vertical lines represents a degree of restoration of calibration accuracy in the dish and cross-dish
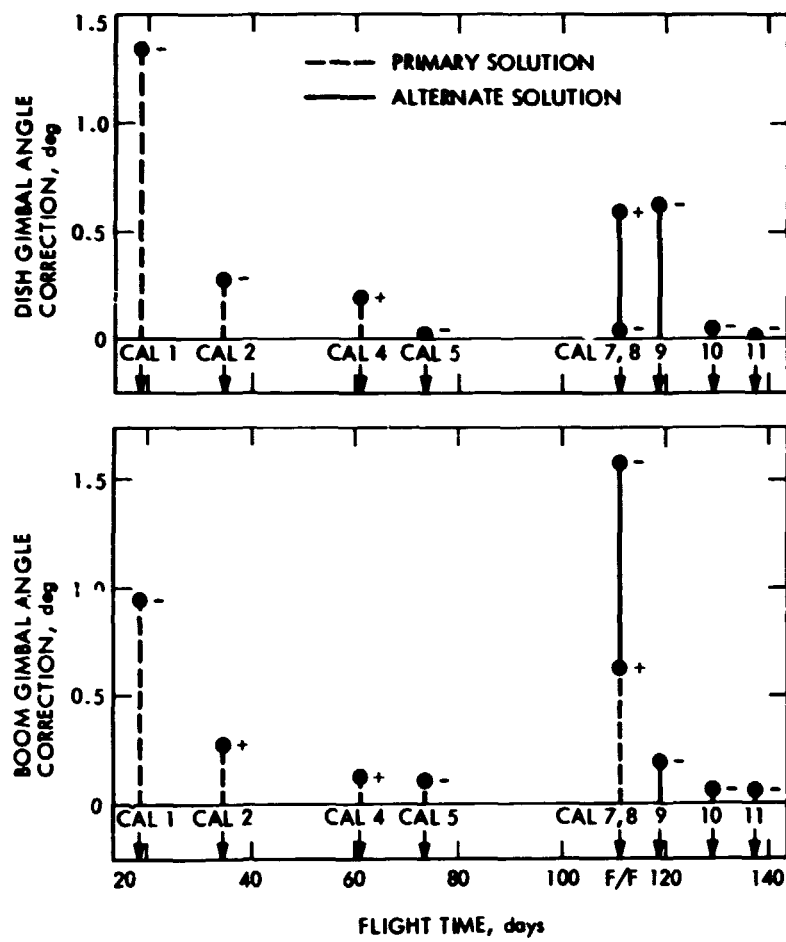
Fig. 9 Gimbaled Actuator Angle Corre... ...on ...
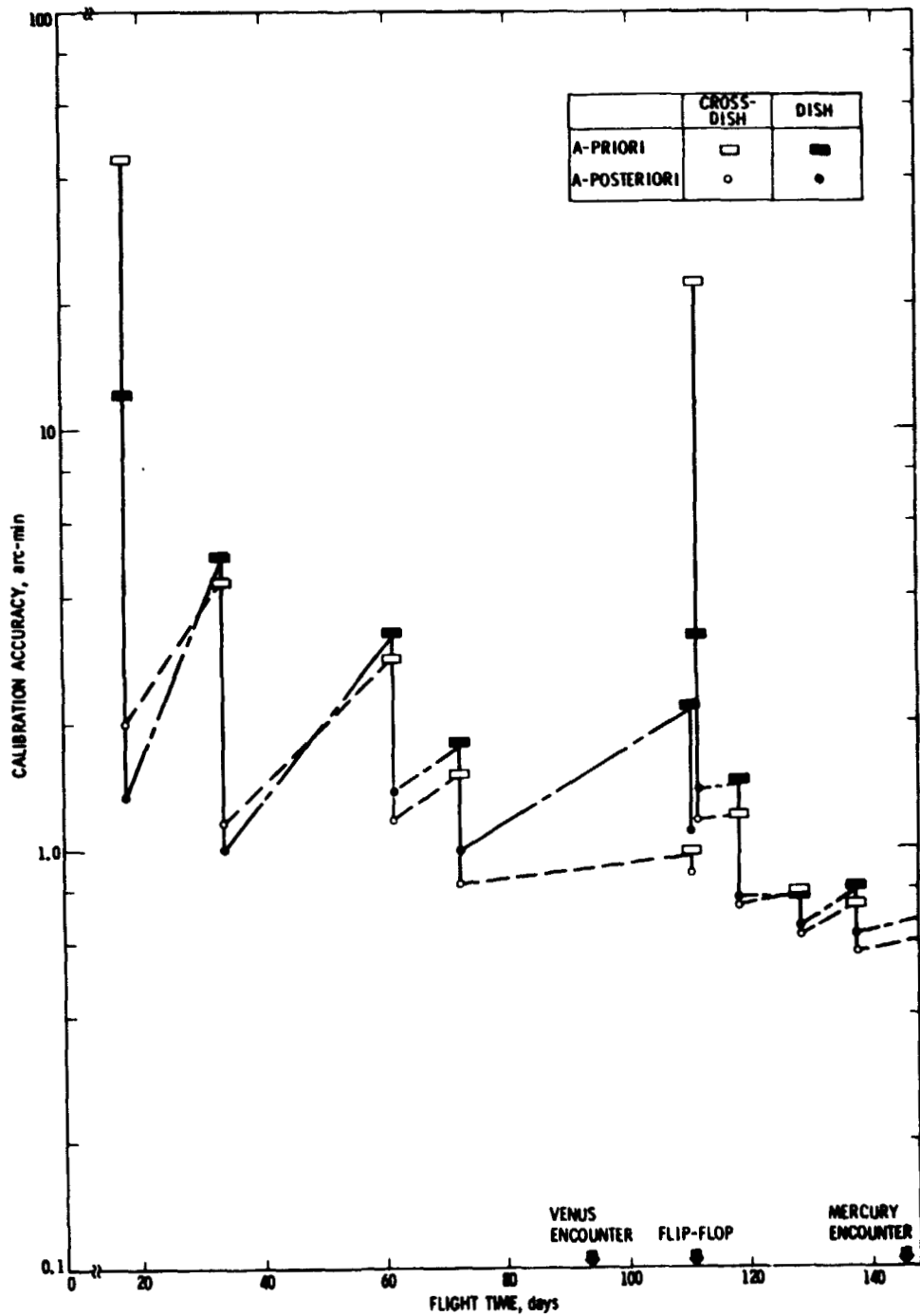from In-Flight Calibrat...

Fig. 10 Time Evolution of HGA Pointing
Calibration Accuracy

(defined as perpendicular to the dish) directions accomplished at each calibration.

The a priori condition with which to start the parameter estimation process was determined based upon the pre-flight calibration results (see Reference 6) of the HGA radiation characteristics and the somewhat degraded values of the APS structure calibration. The degradation was required to account for possible adverse effects due to mechanical shock during launch and boom deployment. The a posteriori condition which had resulted from one calibration was used as the a priori condition of the next except for variance and correlations associated with the signal strength related parameter (z_{11}). The variance of z_{11} was set to 1.0 $(dBm)^2$ and correlations with other parameters to zero to account for large signal strength measurement value change from the preceeding calibration.

The error ellipses associated with calibration accuracy at launch, Venus and Mercury are given in Figure 11. Significant differences in calibration accuracies of the dish and the cross-dish directions were observed at Venus encounter. The resulting uncertainty of HGA pointing in the dish direction was greater than that in the cross-dish direction by almost a factor of 2, while almost identical pointing accuracy in both dish and cross-dish directions was achieved at the Mercury encounter. The explanation for this is (a) that the a priori error ellipse was elongated in dish direction by almost a factor of 3 and (b) that the larger angular range (see Figure 3) covered by the boom actuator than covered by the dish actuator resulted in the higher calibration accuracy in the cross-dish direction.

Table 3 summarizes the estimated error parameters and their accuracies as evaluated a priori and at the calibrations closest to launch, Venus encounter and Mercury encounter. It is seen from the table that almost no improvements on estimating the attitude control subsystem related parameters were made, $(z_1, z_2$ and $z_3)$, while higher accuracy in estimating the parameters relevant to the structure subsystem $(z_4, z_5$ and $z_6)$, the APS subsystem $(z_7, z_8$ and $z_9)$, and the antenna radiation (z_{10}) was achieved. The signal strength related parameter (z_{11}) estimation accuracy was consistently obtained about 0.1 dBm (1σ) except for Calibration 1.
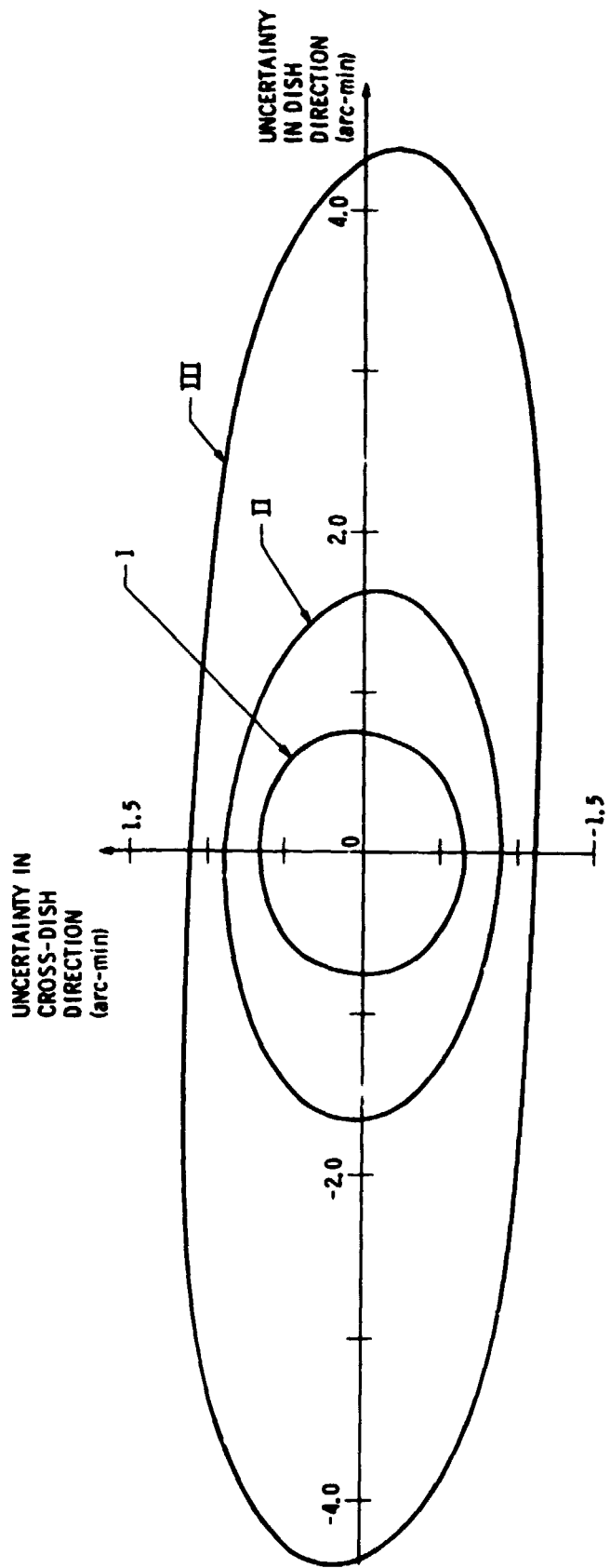
Fig. 11 HGA Pointing Calibration Error Ellipses

I. One-Sigma Error Ellipse at Mercury
Encounter

II. One-Sigma Error Ellipse at Venus
Encounter

III. One-Tenth-Sigma Error Ellipse at
Spacecraft Launch

Table 3 HGA Calibration Results

Parameter Symbol	Unit	A Priori		Calibration 1		Calibration 5		Calibration 11	
		Initial Value	1σ Accuracy	Estimated Value	1σ Accuracy	Estimated Value	1σ Accuracy	Estimated Value	1σ Accuracy
z_1	mrad	0.0	1.5	0.0	1.5	0.0	1.5	10.4	1.4
z_2	mrad	0.0	1.5	0.7	1.5	2.7	1.5	18.2	1.2
z_3	mrad	0.0	0.3	-0.1	0.3	-0.1	0.3	0.1	0.3
z_4	mrad	0.0	3.1	11.1	2.4	10.4	1.4	10.4	0.5
z_5	mrad	0.0	6.6	-6.1	6.1	24.8	1.9	3.3	1.5
z_6	mrad	0.0	3.1	5.5	3.1	1.8	1.8	11.1	1.1
z_7	mrad	0.0	13.1	20.9	5.1	15.0	3.6	35.6	1.2
z_8	mrad	0.0	3.5	1.8	3.4	2.5	3.3	9.8	0.2
z_9	mrad	0.0	3.1	11.4	2.3	5.5	1.5	30.0	0.2
z_{10}	rad^{-1}	90.899	0.010	90.753	0.010	90.430	0.006	90.116	0.004
z_{11}	dBm	0.00	1.00	-119.50	0.27	-133.39	0.13	-148.14	0.10

In the Appendix is given a more complete set of data. It presents estimated error parameters and their accuracies as evaluated at all calibrations.

Table 4 summarizes the worst case HGA total pointing accuracy as a function of mission time for X- and S-band. Data is given for each calibration period. The knowledge type error includes the calibration residual error. The control type error includes the worst case attitude limit cycle motion of the spacecraft, command generation and approximation error and mechanical backlash.

Worst case was selected as the criteria by which to evaluate pointing because, as part of a continuous communication system, HGA pointing is of interest at all times, not just during selected intervals which can be optimized. For this reason, the total pointing error is the sum of all the individual error contributions which can reasonably be expected to occur. In the following discussion, explanation is given for selection of each parameter value as representing worst case, and mention is made of a more likely error value.

The X-band residual calibration error is the mean boresight pointing error remaining after a calibration, as evaluated at the next calibration. This is true except for calibrations 5, 7 and 11. The large geometry change at Venus encounter between calibrations 5 and 7, the flip-flop following 7, and the lack of a calibration after 11 required extrapolation of this error for these three calibrations. Since no S-band calibration per se was performed, the residual S-band error is simply the sum of the residual X-band error and the estimated separation between the two boresights.

The error contributed by the attitude control limit cycle motion is the same for both X-band and S-band. It is assumed that all three axes are simultaneously at their worst 0.25 deg deadband edges. Obviously this is a conservative assumption. If well behaved, two-sided, independent limit cycles in the absence of external torque are assumed, all three axes should simultaneously exceed 0.20 deg error only 0.1% of the time. Considering some flight-observed characteristics such as attitude channel cross-coupling and solar pressure, the true effect of this error most of the time is much less than the value stated in the table.

Table 4 HGA Worst Case Pointing (Deg)

Error Source		Calibration Number									
	a priori	1	2	4	5	7	8	9	10	11
X-band Pointing											
1. Residual Calibration Error	1.65	0.44	0.24	0.16	0.16	0.10	0.67	0.09	0.07	0.07
2. Attitude Limit Cycle Motion	0.28	0.28	0.32	0.37	0.35	0.43	0.43	0.43	0.43	0.37
3. Backlash	0.27	0.27	0.27	0.27	0.27	0.24	0.24	0.22	0.22	0.22
4. Profile Approximation/ Command Update	0.12	0.12	0.12	0.12	0.12	0.12	0.12	0.12	0.12	0.12
5. Command Resolution Error	0.09	0.09	0.09	0.09	0.09	0.09	0.09	0.09	0.09	0.09
Total X-band Pointing Error	2.41	1.20	1.04	1.01	0.99	0.98	1.55	0.95	0.93	0.87
S-band Pointing											
1. Residual Calibration Error	1.87	0.66	0.46	0.38	0.38	0.32	0.89	0.31	0.29	0.29
2. Attitude Limit Cycle Motion	0.28	0.28	0.32	0.37	0.35	0.43	0.43	0.43	0.43	0.37
3. Backlash	0.27	0.27	0.27	0.27	0.27	0.27	0.27	0.27	0.27	0.27
4. Profile Approximation Error	0.90	0.90	0.93	0.95	0.96	0.95	0.95	0.95	0.95	0.95
5. Command Update Error	0.46	0.46	0.47	0.47	0.47	0.47	0.47	0.47	0.47	0.47
6. Command Resolution Error	0.09	0.09	0.09	0.09	0.09	0.09	0.09	0.09	0.09	0.09
Total S-band Pointing Error	3.87	2.66	2.44	2.43	2.42	2.46	3.00	2.42	2.40	2.36

Backlash became a major error contributor on Mariner 10. Actuator
backlash was about 0.16 deg per axis. In addition the structural backlash
inferred from the data of Calibrations 3 through 11 was 0.25 deg in boom and
0.10 deg in dish. Use of Position Mode control minimized the effect of actuator
backlash. The monotonic nature of the cruise pointing profile and judicious
command selection during critical periods further ameliorated the effects of
backlash. However, it is reasonable to assume backlash effects on S-band
and early (before backlash calibration) X-band pointing could have been as large
as 0.27 deg. Backlash effects on later X-band pointing were limited to 0.22 deg.

HGA profile approximation and command update errors are primarily
due to operational constraints. The actuator command profile is a "stairstep"
approximation of a piecewise linear fit to the true Earth pointing direction
as a function of time in boom and dish coordinates. This is illustrated
conceptually in Figure 12. The profile approximation error is the difference
between the true Earth direction and the piecewise fit. It can be minimized
by increasing the number of line segments in the fit. The antenna profile
which was loaded into the spacecraft computer was aimed at providing pointing
accuracies sufficient for S-band communication. Therefore the profile approx-
imation error was allowed to be as large as 0.96 deg during cruise. The command
update error is a function of the frequency of antenna pointing updates. The
more frequent the update, the smaller the update size, until the lower limit
of the actuator step size, 0.125 deg, is reached. The commanded step size
during S-band operations ranged as large as 0.87 in boom and 0.37 deg in dish,
This contributed 0.47 deg error.

The total effect of these two errors was much smaller in X-band.
X-band HGA pointing was optimized at DSN station rise and updated once or
twice. This strategy limited the combined profile and command update error
to 0.12 deg.

The final error source considered is the command resolution error.
Since the step size was 0.125 deg in the Position Mode, the effect of one-half
the step size per axis must be considered. This contributes 0.09 deg error.

To summarize comments with regard to Table 4, the pointing error number
can be adjusted based on assumptions concerning limit cycle motion backlash
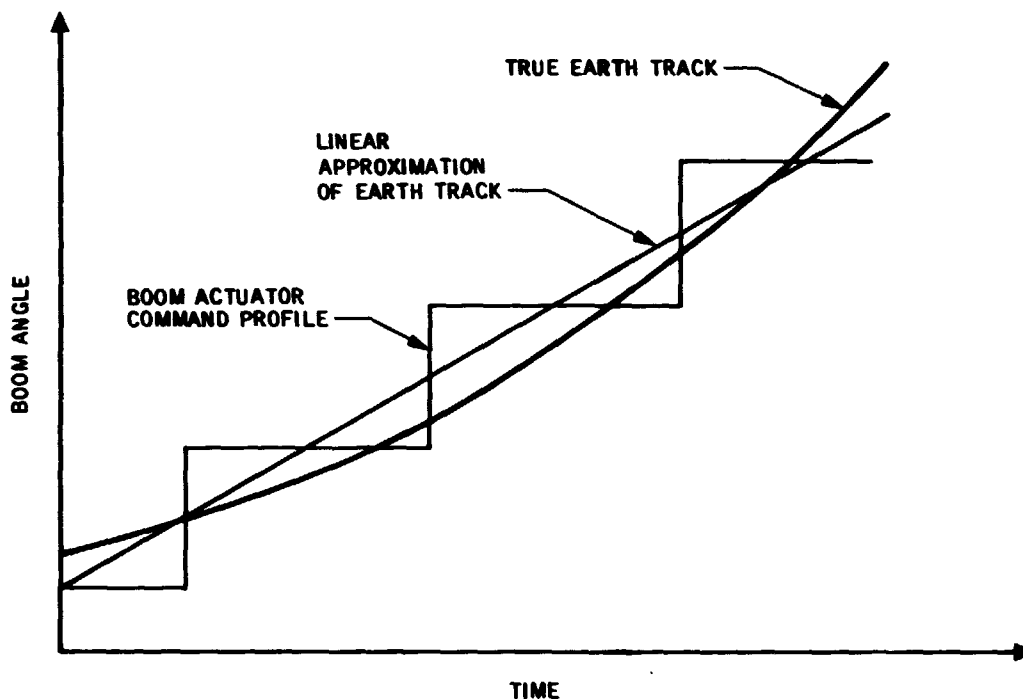effects and command strategy. The total error numbers quoted in the table

Fig. 12   HGA Command Generation Errors

are a fair representation of observed flight performance including worst case limit cycle.

Figure 13 illustrates pointing performance observed at a time when the profile was optimized (Mercury encounter) and the actual affect of limit cycle motion is taken into account. In the figure a limited number of points each representing the difference between the boresight vector and Earth vector is plotted. Estimates of boresight pointing are based on the last calibration ten days earlier. Of the 78 points plotted, only six have pointing error in excess of 0.5 deg. None is greater than 0.7 deg.

Based on the results of the in-flight calibration, the following conclusions can be drawn:

(1)   Feasibility of in-flight calibration of the pointing of a two-axis gimbaled antenna with an X-band transmitter was demonstrated.

(2)   Worst case pointing control accuracy of the antenna was significantly improved with the calibration, from 2.41 deg a priori to 0.87 deg at Mercury encounter.
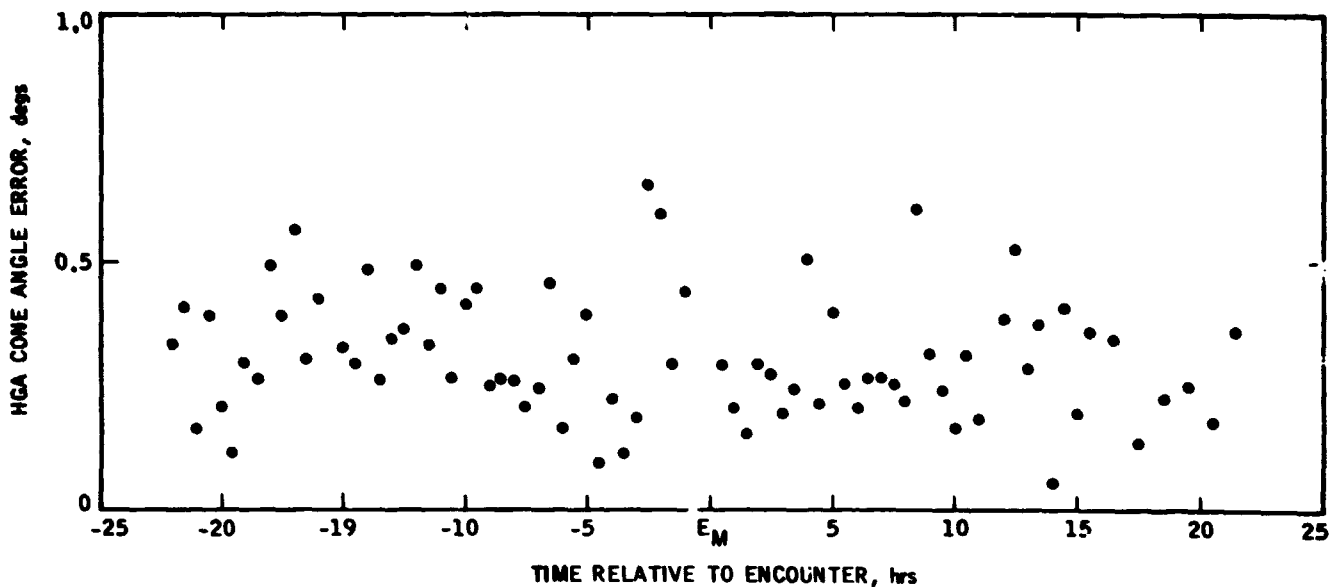
Fig. 13 HGA Pointing Error at Mercury Encounter

(3) The resultant in-flight calibration accuracy can be described by
a 3σ error ellipse whose semi-major axis was reduced from 130
arc-minutes a priori to 5 arc-minutes at Venus encounter and
2 arc-minutes at Mercury encounter.

(4) In order to maintain antenna pointing acceptable to Radio Science
experimenters, it is necessary to implement HGA profile corrections
based on each calibration. Failure to do this on MVM resulted
in degraded X-band data although the pointing for S-band was
acceptable.

(5) The calibration schedule must be flexible enough to allow for
changes necessitated by spacecraft surprises. An example of
this on MVM was the change caused by the discovery of the signifi-
cant backlash.

(6) Hardcopy and tape-recorded station AGC voltage averaged over
five-second intervals should be made available. Analysts trans-
cribed these from a television display. This introduced error
and significantly increased analysis time.

(7) Four working days were required to reduce data from one calibration.

(8) A simple mathematical model was shown to be a sufficiently accurate
representation of the HGA radiation pattern for the main lobe.

APPENDIX

Detailed Calibration Results

In this appendix is given more detailed data on the calibration. Table A1 gives a summary of when the calibration events occurred with respect to significant mission events. Table A2 presents a summary of estimated error parameters and their accuracies as evaluated at each of the calibrations.

Table A1: Calibration Event Summary

Event	Date: Day, Year	Days from Launch	HGA Solution
Launch	307, 1973	0	Primary
Calibration 1	326, 1973	19	Primary
Calibration 2	342, 1973	35	Primary
Calibration 4	4, 1974	62	Primary
Calibration 5	15, 1974	73	Primary
Venus Encounter	36, 1974	94	Primary
Calibration 7	53, 1974	111	Primary
Calibration 8	53, 1974	111	Alternate
Calibration 9	61, 1974	119	Alternate
Calibration 10	71, 1974	129	Alternate
Calibration 11	79, 1974	137	Alternate
Mercury Encounter	89, 1974	147	Alternate

Table A2 Detailed Calibration Results

Parameter Symbol	Unit	A priori		Calibration 1		Calibration 2		Calibration 4		Calibration 5		Calibration 7		Calibration 8		Calibration 9		Calibration 10		Calibration 11	
		Value	Accuracy 1σ	Estimated Value	Accuracy 1σ	Estimated Value	Accuracy 1σ	Estimated Value	Accuracy 1σ	Estimated Value	Accuracy 1σ	Estimated Value	Accuracy 1σ	Estimated Value	Accuracy 1σ	Estimated Value	Accuracy 1σ	Estimated Value	Accuracy 1σ	Estimated Value	Accuracy 1σ
		0.0	1.5	0.5	1.5	2.4	1.5	0.3	1.5	0.0	1.5	7.3	1.5	7.1	1.5	5.3	1.5	8.6	1.4	10.4	1.4
		0.0	1.5	0.7	1.5	1.2	1.5	3.3	1.5	2.7	1.5	13.5	1.5	12.9	1.5	9.6	1.4	13.3	1.4	14.2	1.2
		0.0	0.3	-0.1	0.3	0.0	0.3	-0.1	0.3	-0.1	0.3	0.1	0.3	0.1	0.3	0.1	0.3	0.1	0.3	0.1	0.3
		0.0	3.3	11.1	2.4	0.7	2.2	16.1	1.7	10.4	1.4	-6.3	0.6	-6.6	0.6	-6.1	0.6	-8.5	0.6	10.4	0.5
		0.0	6.6	-4.3	6.1	50.6	2.1	25.6	1.9	24.8	1.9	-8.9	1.6	-7.1	1.5	-6.2	1.5	-4.8	1.5	5.3	1.5
		0.0	3.3	5.5	3.1	2.6	2.8	3.6	2.1	1.8	1.8	-9.8	1.6	-8.3	1.1	-7.5	1.1	-4.9	1.1	11.1	1.1
		0.0	13.1	20.9	5.1	33.7	3.9	12.2	3.6	15.0	3.6	-19.0	3.5	28.4	1.5	24.5	1.5	32.6	1.4	35.6	1.2
		0.0	3.5	1.8	3.4	1.4	3.3	2.7	3.3	2.5	3.3	3.1	3.3	-4.5	0.3	-7.0	0.2	-7.5	0.2	9.8	0.2
		0.0	3.3	11.4	2.3	7.4	2.2	1.6	1.8	5.5	1.5	24.0	0.6	24.4	0.3	28.0	0.2	27.5	0.2	20.0	0.2
		90.099	0.010	90.753	0.010	90.508	0.008	90.438	0.006	90.430	0.006	90.317	0.006	90.317	0.006	90.267	0.005	90.280	0.005	90.116	0.004
		0.00	1.00	-119.50	0.27	-128.65	0.10	-132.08	0.10	-133.39	0.13	-132.44	0.13	-133.95	0.13	-136.99	0.08	-165.11	0.16	-168.16	0.10

REFERENCES

1. "Mariner Venus/Mercury 1973 Spacecraft System Requirements Document", Project
   Document 615-12, Jet Propulsion Laboratory, Pasadena, California, February 14,
   1972, (JPL internal document).

2. Budos, J.D., Folkers, L.K., Hardman, J.M., "Mariner Venus Mercury 1973
   Guidance and Control Functional Description and Block Diagram", Project
   Document 615-120, Jet Propulsion Laboratory, Pasadena, California, April 2,
   1973, (JPL internal document).

3. Brockman, M.H., et al., "DSN Standard Practice: Deep Space Network/Flight
   Project Interface Handbook", 810-5 Revision D, Jet Propulsion Laboratory,
   Pasadena, California (JPL internal document).

4. Folkers, L.K., "Mariner Venus-Mercury 1973 Flight Equipment High Gain Antenna
   Pointing Accuracy Analysis", Project Document 615-111, Jet Propulsion Lab-
   oratory, Pasadena, California, December 1, 1972, (JPL internal document).

5. Edelson, R.E., et al., "Telecommunications Systems Design Techniques
   Handbook", TM 33-571, Jet Propulsion Laboratory, Pasadena, California,
   July 1972.

6. "Mariner Venus/Mercury 1973 Spacecraft Functional Requirements", The Boeing
   Company, Seattle, Washington, October 11, 1971.